Journal of Inorganic and General Chemistry
ZAAC
Zeitschrift für anorganische und allgemeine Chemie
DOI: 10.1002/zaac.202000475
ARTICLE

Molecular magnetic properties of a dysprosium(III) complex coordinated to a nonadentate bispidine ligand

Patrick Cieslik,[a] Peter Comba,*[a, b] Waldemar Hergett,[c] Rüdiger Klingeler,[c, d] Günter Finn Peter Plny,[a] Lena Spillecke,[c] and Gunasekaran Velmurugan[a]

Dedicated to Prof. Dr. Peter Klüfers on occasion of his 70th birthday

The Dy^{III} complex of the nonadentate bispidine L^1 (bispidine = 3,7-diazabicyclo[3.3.1]nonane) has a capped square antiprismatic structure, known to lead to suppressed quantum relaxation of magnetization by quantum tunneling. $[Dy^{III}L^1]OTf$ indeed is an SMM with a modest barrier to magnetization relaxation. The experimentally determined barrier of 46 cm^{-1} is confirmed by *ab initio* calculations (43.5 cm^{-1}), and the quantum-chemical analysis indicates that ligand modifications, leading to a higher symmetry and a stronger axial ligand field should significantly increase the effective barrier to magnetization relaxation.

Introduction

It was in the early 1990ies when the first metal complexes were described that retain magnetization at low temperature for some time when the magnetic field is switched off.[1,2] This quantum phenomenon is of fundamental interest and has a range of possible applications.[2–5] The key feature of SMMs is a high blocking temperature T_B (the temperature below which an SMM retains magnetization for a certain time), and this depends on quantum tunneling of magnetization in the low temperature regime and thermal relaxation described by the anisotropy barrier U_{eff}.[6–10] The historic Mn_{12} SMM has a blocking temperature below 4 K (effective barrier of about 42 cm^{-1}) and therefore primarily is of academic interest.[2] Decisive for blocking of the magnetization is the splitting of the ground state multiplet and this primarily depends on the ligand field and the spin-orbit coupling, and for a suitable SMM the magnetic anisotropy should be axial and the ground states should mainly consist of the $m_s = S$ and -S states.[11,12] Due to the large spin-orbit coupling and a generally large total spin, lanthanide complexes have been in the focus for some time, and a dysprosium(III) sandwich complex (a single ion magnet, SIM) was the first to show a blocking temperature above the liquid helium regime (T_B of 80 K, effective barrier of 1541 cm^{-1}).[13]

Among the methods to compute the electronic ground state, magnetic exchange and relaxation pathways and along these lines to optimize SMMs and predict their performance, a quantum-chemical protocol has been developed that is based on an *ab initio* CASSCF wavefunction and spin-orbit coupling introduced via restricted active space state interaction. This allows to derive the multiplet splitting-for exchange-coupled systems, the Lines model is used to perform a ligand field analysis involving extended Stevens operators.[14–18] This protocol has been used successfully, in particular also for mono- and oligonuclear lanthanide complexes, for which it has been carefully validated by combinations of SQUID magnetometry, EPR and MCD spectroscopy, analyzed by ligand field theory and combined with the *ab initio* protocol.[19,20]

Here we describe the experimental magnetic data and computed multiplet splitting of the Dy^{III} complex of the new nonadentate bispidine ligand L^1, $[Dy^{III}L^1]OTf$ (see Scheme 1 for the structure of the ligand and the complex). The adamantane-derived bispidine platform provides a very rigid scaffold for tetra-, penta- and hexadentate ligands that have been used extensively for various applications in transition metal chemistry.[21–24] The relatively large cavity size[23,24] and the ease to increase the denticity beyond six[24–27] makes these ligands ideal for lanthanides. Since the complexes with the octadentate ligand L^2 were nine-coordinate with a monodentate anion or OH_2 in aqueous solution completing the coordination sphere, we prepared the corresponding nonadentate L^1, also in view of

[a] P. Cieslik, P. Comba, G. F. P. Plny, G. Velmurugan
Universität Heidelberg, Anorganisch-Chemisches Institut, INF 270, 69120 Heidelberg, Germany
Fax: +49-6221-546617
E-mail: peter.comba@aci.uni-heidelberg.de
[b] P. Comba
Interdisziplinäres Zentrum für Wissenschaftliches Rechnen, IWR, Universität Heidelberg INF 270, 69120 Heidelberg, Germany
[c] W. Hergett, R. Klingeler, L. Spillecke
Kirchhoff-Institut für Physik, Universität Heidelberg, INF 227, 69120 Heidelberg, Germany
[d] R. Klingeler
Centre for Advanced Materials (CAM), INF 225, 69120 Heidelberg, Germany

Supporting information for this article is available on the WWW under https://doi.org/10.1002/zaac.202000475

applications as fluorescence sensors with extended excited state life-times.[28]

The structures of $[Ln^{III}L^1]NO_3$ (Ln = Tb, Gd and Yb) and $[Eu^{III}L^1]CF_3CO_2$ are all very similar and are best described as capped square antiprismatic (CSAPR, C_{4v}, see Figure 1). We anticipate that the $[Dy^{III}L^1]$OTf complex discussed here, for which no crystal structural data are available at present, has a very similar molecular structure, and this is confirmed by the analysis of the molecular magnetism. For SMM properties, a square antiprismatic ligand field is of particular interest since this is believed to suppress quantum tunneling of magnetization (QTM).[29]

Results and Discussion

The Dy^{III} complex $[Dy^{III}L^1]$OTf was prepared according to Scheme 1, and the analytically pure compound was isolated as a white solid by ether diffusion into a methanolic solution of the complex. Elemental analysis, HR-mass, HR-ICP-MS and TGA provide information about the purity of the sample and the stoichiometry with respect to co-crystallized solvent (see Experimental Section and Supporting Information).

DC magnetic susceptibility and magnetization

The temperature dependence of the direct current (DC) magnetic susceptibility χ (shown as χT vs. T in Figure 2) was measured on a fixed powder sample of $[Dy^{III}L^1]$OTf in the temperature range between 1.8 K and 300 K in an external static magnetic field of 0.1 T. Upon further increase of the temperatures up to 400 K, the susceptibility data show a small hump around 320 K (see Figure S1). TGA investigations imply, that this hump is due to the loss of one molecule water per formula unit (f.u.) so that the further analysis is restricted to $T < 300$ K.

The room temperature χT value of 13.28 erg K/(mol G^2) is close to the theoretically predicted free-ion value for the $^6H_{15/2}$ configuration, with $g_J = 4/3$, *i.e.*, 14.17 erg K/(mol G^2),[30] and it agrees well with other results for mononuclear Dy^{III} complexes reported in the literature.[19,31,32] With lowering the temperature, χT smoothly decreases until it drops more significantly below about 100 K, reaching a value of 9.91 erg K/(mol G^2) at T = 1.8 K. The decrease in χT can be assigned to the depopulation of energetically higher multiplets with decreasing temperatures as well as the Zeeman splitting induced by the external magnetic field. The drop at lower temperatures is likely due to magnetic anisotropy.

The inset to Figure 2 shows the magnetization measured in external magnetic fields up to 7 T at various isothermal

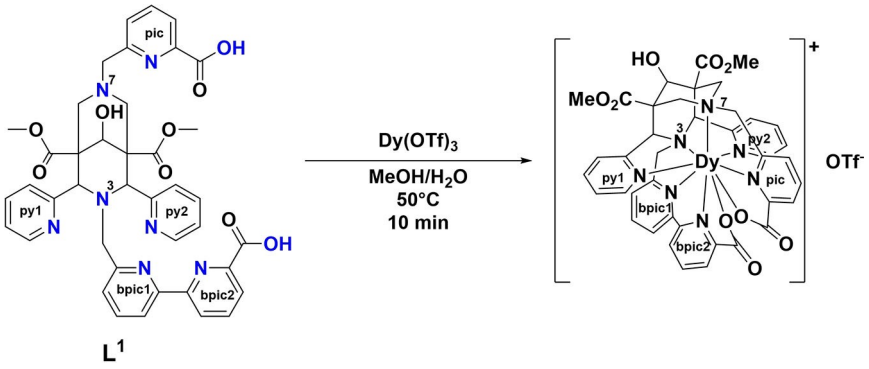

Scheme 1. Reaction of the ligand L^1 with the triflate of Dy^{III} to $[Dy^{III}L^1]$OTf.

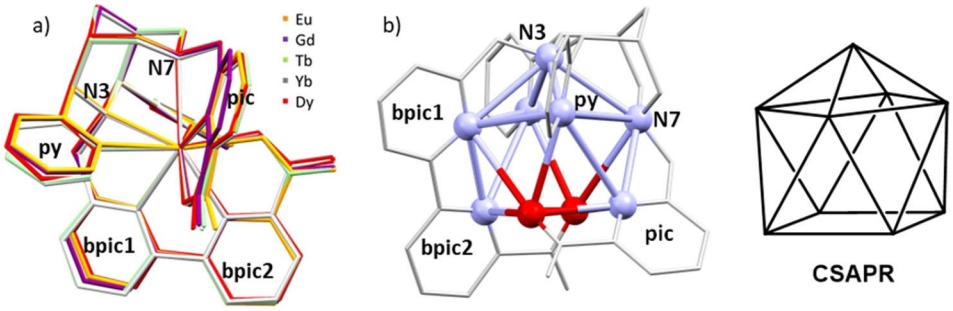

Figure 1. a) Overlay plot of the X-ray structures of the $[Ln^{III}L^1]^+$ complex cations with Ln = Eu, Gd, Tb, Yb, also including the DFT-optimized structure with Ln = Dy. b) Plot of the coordination polyhedron of the Yb complex and sketch of the CSAPR geometry.[28]

conditions. With increasing magnetic field, the magnetization measured at 1.8 K sharply rises to approximately 1 T while it saturates to a linear increase at the highest measured magnetic fields. Extrapolation of the high-field magnetization to zero field yields about 4.5 μ_B/f.u. which is much smaller than the theoretical predicted saturation value for an $m_J = 15/2$ ground state (10 μ_B/f.u.). This observation indicates the presence of low-lying excited states and/or significant influence of magnetic anisotropy, and this is supported by the quantum-chemical analysis (see below and Supporting Information, Tables S3, S4). Both is further witnessed by the linear increase of the M vs. B curve at higher magnetic field without indication of saturation in the accessible field range.[20,33]

AC magnetic susceptibility

To investigate the dynamic magnetic response, alternating current (AC) magnetic susceptibility measurements were performed in a frequency range between 5 Hz–1000 Hz with an AC magnetic field amplitude of 3 Oe. In the absence of static magnetic fields, no out-of-phase signal was observed within the studied temperature range of 1.8 K–20 K (data not shown). We attribute this to a quantum tunneling mechanism (QTM) due to the weak axial ligand field and low overall symmetry of the coordination polyhedron, resulting in transverse anisotropy and therefore mixing of the m_J states.[12] By applying a small external magnetic field of 0.1 T, the QTM is suppressed and field-induced slow relaxation of the magnetization is observed as indicated by the peak in the logarithmically scaled frequency dependence of the out-of-phase (χ'') signal as shown in Figure 3 (b). For further analysis, the χ'' data were fitted using a generalized Debye model[34] as described in Eqn. S1. The obtained relaxation times τ are shown as an Arrhenius plot in Figure 4 (a).

In the Arrhenius plot of the obtained relaxation times (Figure 4 (a)), two different linear regimes separated by a kink at around T = 4 K are visible, which indicate the presence of two different effective energy barriers U_{eff}.[35,36] Fitting the obtained relaxation times by means of the Arrhenius law:

$$\tau = \tau_0 exp\left(-U_{eff}/k_B T\right) \quad (1)$$

where τ_0 is a constant prefactor and k_B the Boltzmann constant, yields the effective energy barriers $U_{eff,1} = 31.4(5)$ K (21.8(3) cm^{-1}; $\tau_{0,1} = 2.9\,e{-}5$ s) and $U_{eff,2} = 66.2(5)$ K (46.0(3) cm^{-1}; $\tau_{0,2} = 2.5\,e{-}8$ s) in the two regimes. Note, that in the literature often a combination of Orbach, Raman and direct processes is used,[10] which however fails qualitatively and quantitatively to describe the data at hand.

The presence of two energy barriers is not only signaled by the different regimes in the temperature dependence of the relaxation times but also by the temperature dependence of the eccentricity parameter α (see SI for further information). The parameter α is a measure of the distribution of relaxations times τ so that α close to zero implies the presence of only one dominating relaxation process. While α, shown in Figure 4 (b), is rather small and constant at higher temperatures, indicating a

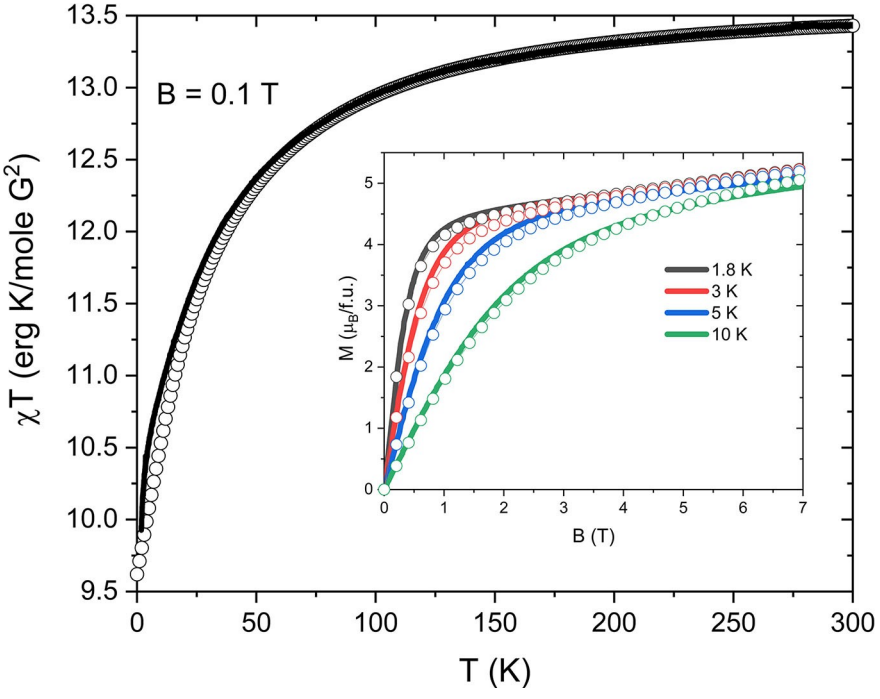

Figure 2. Temperature dependence of the DC susceptibility measured in an external magnetic field of 0.1 T. Inset: Magnetic field dependence of the dc magnetization measured at various constant temperatures. The solid lines are experimental data, the open circles are simulated data from the quantum chemical calculations, see below.

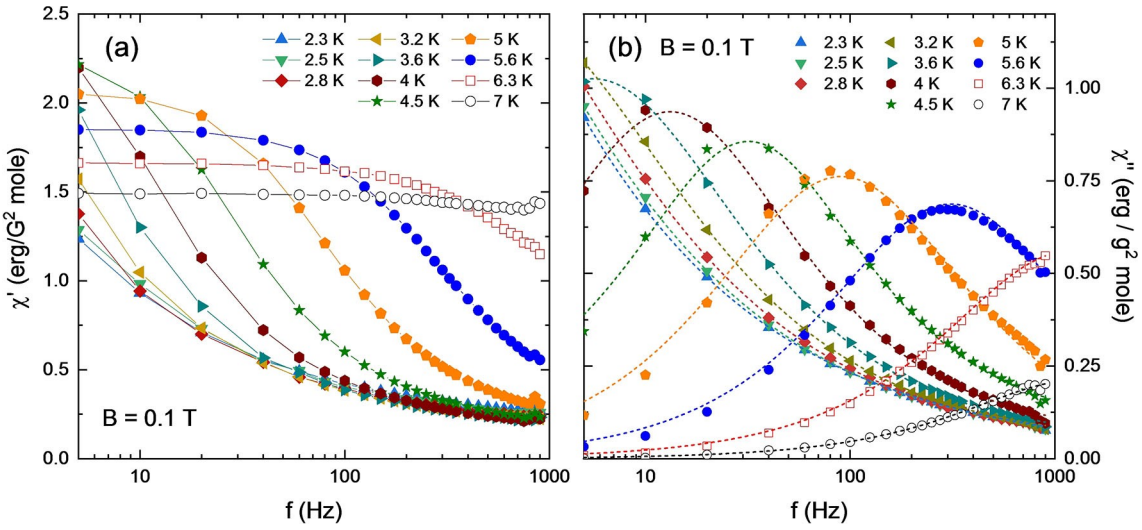

Figure 3. In-phase (a) and out-of-phase (b) AC magnetic susceptibility of [$Dy^{III}L^{1}$]OTf measured in an external static magnetic field of 0.1 T at several constant temperatures. Dashed lines in (b) correspond to fits using the generalized Debye model (see the main text and the SI).

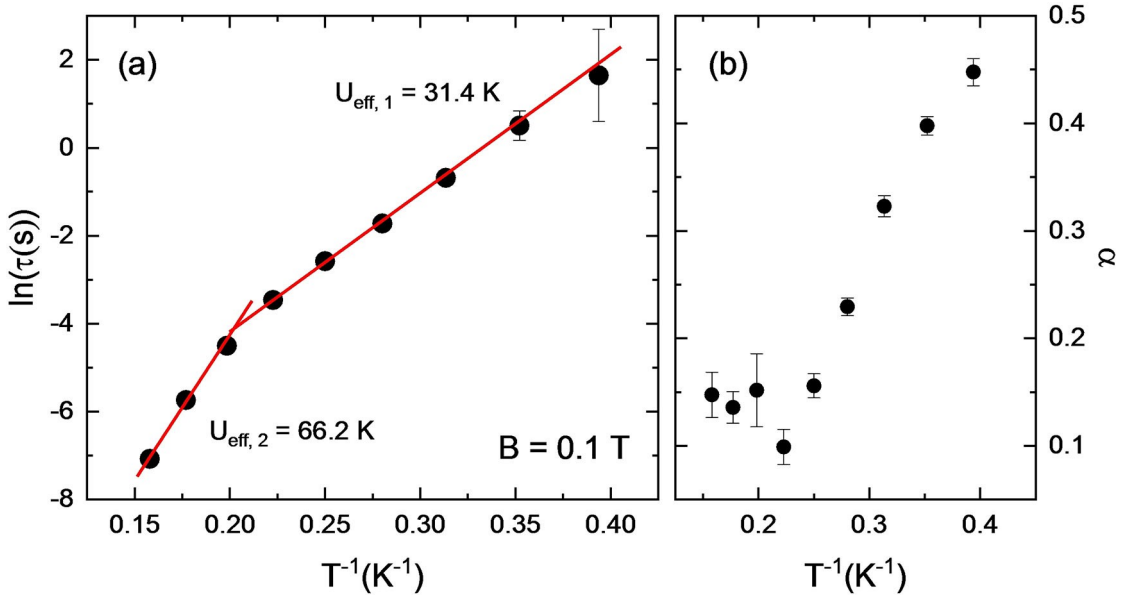

Figure 4. (a) Arrhenius plot of the relaxation times obtained from fitting of the AC susceptibilities (see Figure 3 (b)) of [$Dy^{III}L^{1}$]OTf obtained in an external magnetic field of 0.1 T. (b) Temperature dependence of the fit parameter α (see the SI for more information).

single dominant relaxation process characterized by one energy barrier or time scale, it strongly increases upon cooling below 4 K (please note the inverse scaling of the x-axis). This increase of α signifies the evolution of (at least) a second relaxation process associated with a smaller timescale, i.e., a second relaxation barrier as also directly visible in the Arrhenius plot of the relaxation times in Figure 4(a).

Note, that in general also intermolecular interactions can give rise to magnetic barriers. However, the DC susceptibility and magnetization measurements exclude the presence of significant intermolecular interaction on energy scales larger than 2 K. We hence conclude that the observed relaxation barriers are of purely molecular origin. The presence of two unequivalent molecules in the unit cell could also explain the two different pathways.[37]

Ab initio quantum chemical analysis

The structure of the molecular cations $[Ln^{III}L^{1}]^{+}$ was refined by DFT from the experimental coordinates of the structurally analyzed Tb^{III} complex,[28] and the ground state wavefunction and multiplet splitting were analyzed as described in the Introduction (see Experimental Section and Supporting Informa-

tion for details). The eight Kramers doublets (KDs) of $[Dy^{III}L^1]^+$, corresponding to the $^6H_{15/2}$ ground state, span an energy range of 379 cm^{-1} (Table 1). There is an energy gap of 43.5 cm^{-1} between the ground and the first excited state KD. The ground state (mainly $m_J = \pm 15/2$) shows a relatively strong magnetic anisotropy with a relatively large value for g_{zz} (18.093) and relatively small non-axial terms ($g_{xx} = 0.090$, $g_{yy} = 0.240$). However, this is not a real Ising-type ground state ($g_{xx} \neq g_{yy} \neq 0$). The higher energy KDs (KD 2 to KD 5) also have a high degree of axiality but the g_{zz} values are significantly lower than in the ground state.

The decrease of axial character of the higher energy KDs is due to a large transverse anisotropy contribution. The g_{zz} values are reduced to less than 15 with relatively large values for g_{xx} and g_{yy}. The matrix elements for the transition magnetic moments between the two states of one KD (QTM or TA-QTM, *i.e.* thermally assisted QTM for the higher KDs, see Figure 5) indicate that the ground state KD shows significant transverse anisotropy, and this suggests that significant QTM happens in the ground state itself. This emerges from significant mixing of the excited states $m_J = |\pm 13/2>$, $m_J = |\pm 11/2>$, and $m_J = |\pm 7/2>$ with the ground states $m_J = |\pm 15/2>$. The most efficient excited state quantum tunneling is predicted for KD 3. It follows that reduced axial symmetry leads to instability in the SMM due to TA-QTM. Significant tunneling at the excited KDs suggests TA-QTM via the first and second excited states at 43.5 cm^{-1} and 92.2 cm^{-1}.

Reasons for the decrease in axiality of the higher energy KDs are a decrease of the ligand field symmetry and a comparatively small axial ligand field strength, leading to a deviation of the g tensor axis in the higher energy states. The direction of g_{zz} is largely determined by the donors with the highest electron density. For the ground state KD the g_{zz} axis therefore is oriented towards the two oxygen donors, and this is approx. the direction of the molecular symmetry axis (see Figure 6). In the first excited KD the g_{zz} vector is at an angle of 49.7° with the g_{zz} vector of the ground state, and for the second excited state the deviation from the ground state increases to 52.4°. Therefore, Orbach relaxation (pathway to an opposite m_s state of the next higher KD) increases for KD 3 to 4 (1.718) from KD 2 to 3 (1.008) and KD 1 to 2 (0.175, see Figure 5; see

Table 1. CASSCF + RASSI-SO-computed g tensors and relative energies of the eight lowest energy KDs of $[Dy^{III}L^1]^+$ along with deviations from the principal magnetization axis of the first KD.

nergy (cm^{-1})	g_{xx}	g_{yy}	g_{zz}	θ
0	0.0904	0.2396	18.0929	
43.502	1.1313	1.4128	14.8731	49.7
92.227	3.9227	5.1306	11.3457	52.4
145.385	0.3889	2.8836	13.6419	112.8
174.519	1.2441	2.9467	12.6745	76.5
246.762	1.0008	2.5269	13.5452	48.0
307.687	1.6799	3.0838	13.0739	82.3
378.621	0.2599	0.4014	17.3093	81.1

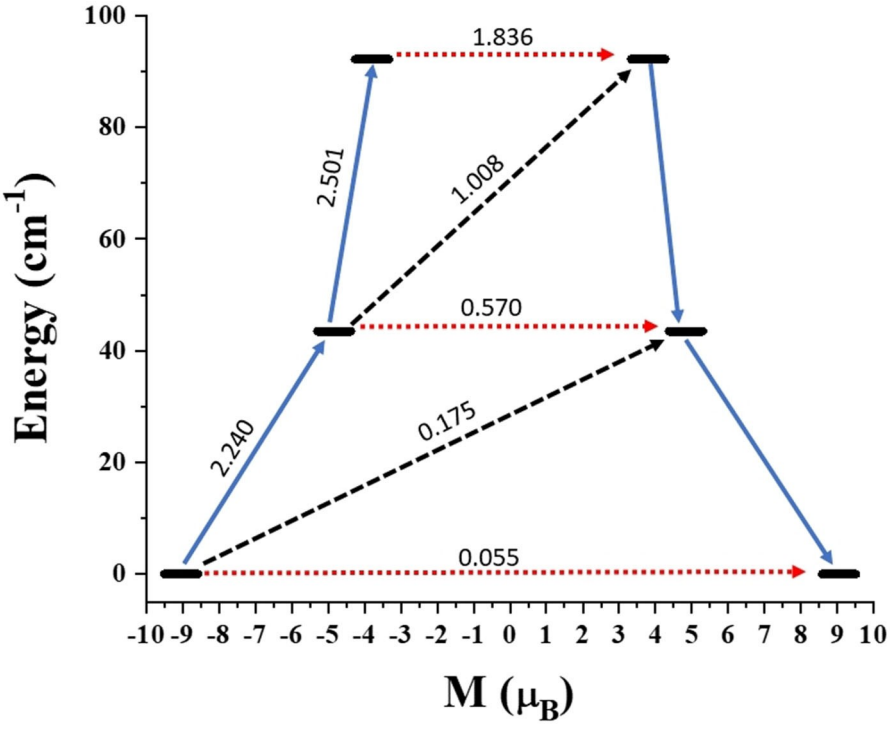

Figure 5. *Ab initio* calculated relaxation dynamics for the Dy^{III} complex. The thick black lines are the Kramers doublets as a function of the magnetic moment. The dashed black lines show possible Orbach pathways. The blue lines are the most probable relaxation pathways for magnetization reversal, and the dotted red lines represent the presence of QTM/TA-QTM between the connecting pairs. The numbers at each arrow are the mean absolute values for the corresponding matrix element of the transition magnetic moment.

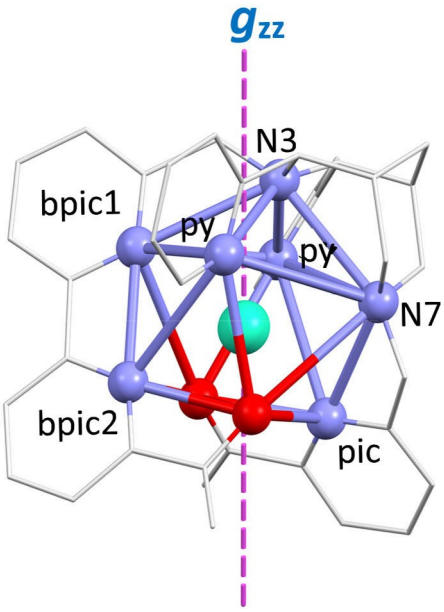

Figure 6. CASSCF computed g_{zz} orientation of the ground state of $[Dy^{III}L^1]^+$ (H atoms and substitution in the ligands are omitted for clarity).

Supporting Information for more details and additional relaxation pathways).

The protocol used to compute the multiplet splitting (see Introduction) also allows to compute the crystal field Hamiltonian. It has been shown that the resulting ligand field parameters and relative energies of the Kramers doublets, specifically for this type of mononuclear Dy^{III} complexes, are very accurate.[20] The computed barriers to the two first excited Kramers doublets (43.5 cm^{-1} and 92.2 cm^{-1}) showing up in the relaxation process is in excellent agreement with the experimental observations. Furthermore, while the calculated magnitudes of the energy barriers are slightly larger than the experimental ones, the ratio between them ($U_{eff,1}/U_{eff,2}$) perfectly coincides.

Conclusion

Among the few nine-coordinate lanthanide SIMs, $[Dy^{III}L^1]^+$ has excellent SMM properties but with respect to other Dy^{III} compounds these are modest at most. The capped square antiprismatic structure seems to be ideal.[32] However, distortions to relatively low overall symmetry and a too weak axial ligand field lead to rather efficient quantum tunneling pathways. Moderate structural variations of the ligand might lead to competitive bispidine-Dy^{III} SMMs, and predictions based on DFT-derived structural modeling, followed by an *ab initio* prediction of the magnetic properties as described here are an interesting possibility to achieve this goal.

Experimental Section

Syntheses. The synthesis of the ligand has been described before, and the general procedure for the complex syntheses is derived from published work:[28] $Dy(OTf)_3$ (34.5 µmol, 1.0 equiv., 20.9 mg) was dissolved in 2 ml of a 1:1 MeOH/H_2O mixture and was combined with a solution of the bispidine L^1 (30.0 mg, 34.5 µmol, 1.0 equiv., in 2 ml MeOH). The mixture was stirred for 10 min at 50 °C, then cooled to ambient temperature, before removing the solvent in vacuo. The solid was recrystallized from an EtOH solution, layered with Et_2O, producing $[DyL^1]OTf \cdot 1.5H_2O \cdot MeOH$ as colorless solid in 23% yield (9.00 mg, 8.03 µmol). HRMS (ESI), calcd for $C_{40}H_{35}DyN_7O_9^+$: 921.1788 $[M]^+$; found: 921.1800; elemental analysis calcd (%) for $C_{42}H_{42}DyF_3N_7O_{14.5}S$: C 45.07, H 3.69, N 8.76; found: C 45.13, H 3.91, N 8.98; HR-ICP-MS: calcd (%) for $C_{42}H_{42}DyF_3N_7O_{14.5}S$: Dy 15.20, found: Dy 14.28.

Magnetism. DC and AC magnetic data were measured using a MPMS3 SQUID magnetometer from Quantum Design equipped with a 7 T magnet. The powder samples were fixed with eicosane in order to avoid orientation or motion of the crystallites in the external magnetic field. The data were corrected by the background of the used sample holder and the diamagnetic contribution of the sample using Pascal's constants.[38]

Computational Details. The density functional theory (DFT) calculations were performed using the ORCA software.[39] The BP86 functional was used in conjunction with the SARC – ZORA-TZVP basis set for Ln, ZORA-def2-TZVP(-f) for the coordinating atoms (O and N) and ZORA-def2-SVP for the rest of the elements. All *ab initio* calculations were implemented by using OpenMOLCAS 19.11.[40] MOLCAS is a quantum chemistry package based on a multiconfigurational approach. Relativistic aspects were included in MOLCAS by the Douglas-Kroll Hamiltonian. Basis sets for all atoms were taken from the ANO-RCC[42] library, specifically: for Dy ANO-RCC 8s7p5d3f2g1h, for atoms close to the lanthanide the VTZ-basis, which means N: ANO-RCC 4s3p2d1f; O: ANO-RCC 4s3p2d1f; for the more distant atoms the very small VDZ-basis, i.e., for C: ANO-RCC 3s2p, for H ANO-RCC 2s. For Dy complete active space self-consistent field (CASSCF) calculations were performed (ground-state atomic multiplicity is $^6H_{15/2}$, which results in eight low-lying Kramers doublets). The CASSCF calculation comprises an active space of nine active electrons in the seven active orbitals, CAS (9,7), hence 21 sextets were considered. The RASSI-SO (restricted active space state interaction - spin orbit)[16] module was used to mix the spin-free states and to consider the spin-orbit effects. In the last step the SINGLE_ANISO code[15,41] implemented in the MOLCAS was used to compute the g-tensors of Dy^{III}.

Acknowledgements

Financial support by the German Science Foundation (DFG), partly under Germany's Excellence Strategy EXC2181/1-390900948 (the Heidelberg STRUCTURES Excellence Cluster), by the German Federal Ministry of Education and Research (BMBF) via the SpinFun project (13XP5088) and by Heidelberg University are gratefully acknowledged. This study was conducted within the Max Planck School Matter to Life, supported by the BMBF in collaboration with the Max Planck Society. We are grateful for computational resources provided by the bwForCluster JUSTUS, funded by the Ministry of Science and the Universities of Baden-Württemberg, Germany, within the framework program bwHPC-C5. L.S. acknowledges support by

the Max-Planck School IMPRS-QD. Open access funding enabled and organized by Projekt DEAL.

[1] T. Lis, *Acta Crystallogr. Sect. B* **1980**, *36*, 2042.
[2] R. Sessoli, D. Gatteschi, A. Caneschi, M. A. Novak, *Nature* **1993**, *365*, 141–143.
[3] R. Sessoli, H.-L. Tsai, A. R. Schake, S. Wang, J. B. Vincent, K. Folting, D. Gatteschi, G. Christou, D. N. Hendrickson, *J. Am. Chem. Soc.* **1993**, *115*, 1804–1816.
[4] L. Bogani, W. Wernsdorfer, *Nat. Mater.* **2008**, *7*, 179–186.
[5] M. Manoli, A. Collins, S. Parsons, A. Candini, M. Evangelisti, E. K. Brechin, *J. Am. Chem. Soc.* **2008**, *130*, 11129.
[6] S. T. Liddle, J. van Slageren, *Chem. Soc. Rev.* **2015**, *44*, 6655.
[7] J.-L. Liu, Y.-C. Chen, M.-L. Tong, *Chem. Soc. Rev.* **2018**, *47*, 2431.
[8] B. Yin, C.-C. Li, *Phys. Chem. Chem. Phys.* **2020**, *22*, 9923.
[9] D. Aravena, E. Ruiz, *Dalton Trans.* **2020**, *49*, 9916.
[10] A. Castro-Alvarez, Y. Gil, L. Llanos, D. Aravena, *Inorg. Chem. Front.* **2020**, *7*, 2478–2486.
[11] J. D. Rinehart, J. R. Long, *Chem. Sci.* **2011**, *2*, 2078–2085.
[12] A. Upadhyay, S. K. Singh, C. Das, R. Mondol, S. K. Langley, K. S. Murray, G. Rajaraman, M. Shanmugam, *Chem. Commun.* **2014**, *50*, 8838–8841.
[13] F.-S. Guo, B. M. Day, Y.-C. Chen, M.-L. Tong, A. Mansikkamäki, R. A. Layfield, *Science* **2018**, *362*, 144–1403.
[14] A. Ceulemans, L. F. Chibotaru, G. A. Heylen, K. Pierloot, L. G. Vanquickenborne, *Chem. Rev.* **2000**, *100*, 787–806.
[15] L. F. Chibotaru, L. Ungur, *J. Chem. Phys.* **2012**, *137*, 064112–064111–064112–064122.
[16] P.-A. Malmqvist, B. O. Roos, B. Schimmelpfennig, *Chem. Phys. Lett.* **2002**, *357*, 230–240.
[17] M. E. Lines, *J. Chem. Phys.* **1971**, *55*, 2977–2984.
[18] C. Rudowicz, *J. Phys. C* **1985**, *18*, 1415–1430.
[19] P. Comba, M. Großhauser, R. Klingeler, C. Koo, Y. Lan, D. Müller, J. Park, A. Powell, M. Riley, H. Wadepohl, *Inorg. Chem.* **2015**, *54*, 11247–11258.
[20] P. Comba, L. J. Daumann, R. Klingeler, C. Koo, M. J. Riley, A. E. Roberts, H. Wadepohl, J. Werner, *Chem. Eur. J.* **2018**, *24*, 5319–5330.
[21] P. Comba, B. Nuber, A. Ramlow, *J. Chem. Soc. Dalton Trans.* **1997**, 347–352.
[22] P. Comba, A. Lienke, *Inorg. Chem.* **2001**, *40*, 5206–5209.
[23] C. Bleiholder, H. Börzel, P. Comba, R. Ferrari, A. Heydt, M. Kerscher, S. Kuwata, G. Laurenczy, G. A. Lawrance, A. Lienke, B. Martin, M. Merz, B. Nuber, H. Pritzkow, *Inorg. Chem.* **2005**, *44*, 8145–8155.
[24] P. Comba, M. Kerscher, K. Rück, M. Starke, *Dalton Trans.* **2018**, *47*, 9202–9220.
[25] P. Comba, U. Jermilova, C. Orvig, B. O. Patrick, C. F. Ramogida, K. Rück, C. Schneider, M. Starke, *Chem. Eur. J.* **2017**, *23*, 15945–15956.
[26] N. Choudhary, A. Dimmling, X. Wang, L. Southcott, V. Radchenko, B. O. Patrick, P. Comba, C. Orvig, *Inorg. Chem.* **2019**, *58*, 8685–8693.
[27] F. Bruchertseifer, P. Comba, B. Martin, A. Morgenstern, J. Notni, M. Starke, H. Wadepohl, *ChemMedChem.* **2020**, *15*, 1591–1600.
[28] L. Abad-Galan, P. Cieslik, P. Comba, M. Gast, O. Maury, L. Neupert, A. Roux, H. Wadepohl, *Chem. Eur. J.*, accepted 2021, DOI: 10.1002/chem.202005459R2.
[29] S. Sakaue, A. Fuyuhiro, T. Fukuda, N. Ishikawa, *Chem. Commun.* **2012**, *48*, 5337.
[30] J. Tang, P. Zhang, *Lanthanide Single Molecule Magnets* **2015**, Springer Verlag, Berlin.
[31] R. Marx, F. Moro, M. Dörfel, L. Ungur, M. Waters, S. D. Jiang, M. Orlita, J. Taylor, W. Frey, L. F. Chibotaru, J. van Slageren, *Chem. Sci.* **2014**, *5*.
[32] N. Ishikawa, M. Sugita, T. Okubo, N. Tanaka, T. Iino, Y. Kaizu, *Inorg. Chem.* **2003**, *42 (7)*, 2440–2446.
[33] P. Ma, F. Hu, R. Wan, Y. Huo, D. Zhang, J. Niu, J. Wang, *J. Mater. Chem.* **2016**, *4*, 5424–5433.
[34] D. Gatteschi, R. Sessoli, J. Villain, *Molecular Nanomagnets*, Oxford University Press, Oxford, **2006**.
[35] Y. Peng, V. Mereacre, C. E. Anson, A. K. Powell, *Dalton Trans.* **2017**, *46*, 5337–5343.
[36] K. C. Mondal, A. Sundt, Y. Lan, G. E. Kostakis, O. Waldmann, L. Ungur, L. F. Chibotaru, C. E. Anson, A. K. Powell, *Angew. Chem. Int. Ed.* **2012**, *51*, 7550–7554; *Angew. Chem.* **2012**, *124*, 7668–7672.
[37] A. A. Patrascu, M. Briganti, S. Soriano, S. Calancea, R. A. Allao Cassaro, F. Totti, M. G. F. Vaz, M. Andruh, *Inorg. Chem.* **2019**, *58*, 13090–13101.
[38] G. A. Bain, J. F. Berry, *J. Chem. Educ.* **2008**, *85*, 532.
[39] F. Neese, *Computational Molecular Science*, Wiley Interdisciplinary Reviews, **2018**, *8*, e1327.
[40] I. Fdez Galvan, M. Vacher, A. Alavi, C. Angeli, F. Aquilante, J. Autschbach, J. J. Bao, S. I. Bokarev, N. A. Bogdanov, R. K. Carlson, L. F. Chibotaru, J. Creutzberg, N. Dattani, M. G. Delcey, S. S. Dong, A. Dreuw, L. Freitag, L. M. Frutos, L. Gagliardi, F. Gendron, A. Giussani, L. Gonzalez, G. Grell, M. Guo, C. E. Hoyer, M. Johansson, S. Keller, S. Knecht, G. Kovacevic, E. Kaellman, G. Li Manni, M. Lundberg, Y. Ma, S. Mai, J. P. Malhado, P. A. Malmqvist, P. Marquetand, S. A. Mewes, J. Norell, M. Olivucci, M. Oppel, Q. M. Phung, K. Pierloot, F. Plasser, M. Reiher, A. M. Sand, I. Schapiro, P. Sharma, C. J. Stein, L. K. Soerensen, D. G. Truhlar, M. Ugandi, L. Ungur, A. Valentini, S. Vancoillie, V. Veryazov, O. Weser, T. A. Wesolowski, P.-O. Widmark, S. Wouters, A. Zech, J. P. Zobel, R. Lindh, *J. Chem. Theory Comput.* **2019**, *15*, 5925–5964.
[41] B. O. Roos, R. Lindh, P.-A. Malmqvist, V. Veryazov, P.-O. Widmark, *J. Phys. Chem. A* **2004**, *108*, 2585.
[42] L. F. Chibotaru, *Adv. Chem. Phys.* **2013**, *153*, 397–519.

Manuscript received: December 23, 2020
Revised manuscript received: February 26, 2021
Accepted manuscript online: March 1, 2021

ARTICLE

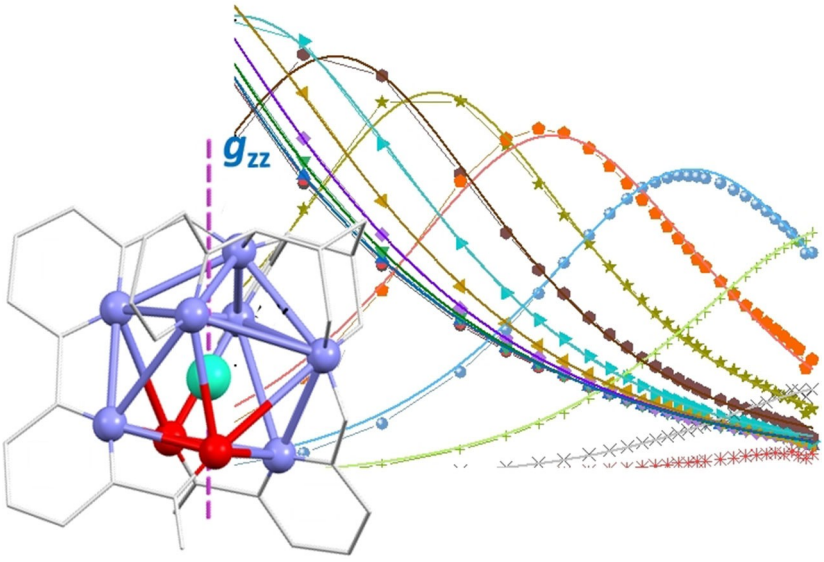

P. Cieslik, P. Comba, W. Hergett, R. Klingeler, G. F. P. Plny, L. Spillecke, G. Velmurugan*